IOP Publishing Measurement Science and Technology
Meas. Sci. Technol. 31 (2020) 045401 (13pp) https://doi.org/10.1088/1361-6501/ab4e50

Joint weighted least squares for normal decomposition of 3D measurement surface

Haoran Xie[1], Fu Lee Wang[2], Qiong Wang[3], Mingqiang Wei[2,5], Reggie Kwan[2] and Jing Qin[4]

[1] The Education University of Hong Kong, Hong Kong, People's Republic of China
[2] The Open University of Hong Kong, Hong Kong, People's Republic of China
[3] Guangdong Provincial Key Laboratory of Computer Vision and Virtual Reality Technology, SIAT, CAS, Shenzhen, People's Republic of China
[4] The Hong Kong Polytechnic University, Hong Kong, People's Republic of China

E-mail: mingqiang.wei@gmail.com

Received 2 May 2019, revised 11 September 2019
Accepted for publication 16 October 2019
Published 6 January 2020

Abstract

3D optical and laser measurement devices can obtain the digital representation of physical objects by boundary surface meshes. Such a representation, however, has no semantic information to describe the object's basic shape and its geometric details individually. Meanwhile, existing mesh filters, which process surface normals as signals defined on the Gauss sphere, mainly deal with noise corrupted by measurement and computational errors. While useful in that they preserve geometric structures, they are not intended for filtering out geometric details whose scales are much larger than that of noise. We assume that a 3D surface contains three geometric properties, i.e. geometric detail, structural pattern, and smooth-varying shape, and consider normals as surface signals defined over both the input mesh and the underlying surface of this mesh. We propose a *joint weighted least squares* (JWLS) to solve the challenging problem of how to filter out the detailed appearance (geometric details) and preserve intrinsic geometric properties (structural patterns) of any measurement surface simultaneously. Specifically, we first suppress high-contrast detail normals, and then detect salient feature normals to produce a feature-guided normal field, and finally jointly fit the original shape. We have shown that a variety of geometric processing tasks benefit from our JWLS, e.g. detail-preserving bas-relief modeling, detail-free mesh smoothing, and detail-enhancing Laplacian coating.

Keywords: mesh smoothing, surface geometry, bas-relief modeling, 3D measurement surface

(Some figures may appear in colour only in the online journal)

1. Introduction

3D optical and laser measurement devices are now affordable [1], which contribute to a variety of advanced applications, such as virtual assembly [2], defect geometry detection [3], 3D printing and manufacturing [4], and autonomous vehicle navigation [5]. However, current 3D scanners lead to the mesh representation of a 3D model with no semantic information to describe its geometric textures and structures separately [6]. This introduces distortions of geometric textures in reverse engineering when applying geometric modeling operations [7] and runs the risk of the destruction of object design [8, 9].

Geometric features comprise abundant details of surface meshes for physical objects [10]. Generally, small-scale features indicate the detailed appearance of surfaces while medium- and large-scale features characterize intrinsic geometric properties of surfaces [11]. Surface decomposition can lead to better understanding of the underlying geometry for shape processing and analysis.

Unlike exsiting mesh filters [12–14] which process surface normals as geometry signals defined on the Gauss sphere, we, inspired by shape analysis in [15], assume that a

[5] Author to whom any correspondence should be addressed.

Figure 1. We list three kinds of geometric processing that benefit from our decomposed normal layers of measurement surfaces. The first is mesh smoothing which produces a detail-free base surface (right) from the corresponding detail-rich model (left). The second is Laplacian coating which enhances the model's geometry (right) by inputting an over-smoothing model (left). The third is bas-relief modeling which produces a detail-preserving bas-relief (right) from a planar mesh equipped with normals (left).

complex surface contains three geometric properties, i.e. geometric detail, structural pattern, and smooth-varying shape. Geometric details (small-scale features) represent the detailed appearance of an object, and structural patterns and smooth-varying shape contribute to control the boundary of geometric structures (medium- and large-scale features) and the overall shape of local surface regions, respectively. Therefore, we can naturally consider surface normals as geometry signals defined over both the original (input) mesh and the underlying surface of this mesh. This allows the design of a novel joint weighted least squares that depends on both shape constraints provided by the original mesh and smooth constraints provided by the underlying mesh.

While the weighted least squares (WLS) model is a fundamental optimization framework that has been widely used in image processing [15–18], there is very little work on leveraging this model for 3D measurement surfaces. This is despite the fact that 3D scanners and depth cameras greatly simplify the geometric modeling process [19], and 3D surfaces become widespread and have myriad applications.

Based on our new geometry assumption, we propose a novel 3D joint WLS algorithm or simply JWLS for decoupling a mesh normal field to a *base layer* and a *detail layer*. Multiple geometric processing tasks benefit from our decomposed two normal layers (see figure 1). For example, (1) we can produce a detail-free mesh smoothing result which matches the base normal field only; (2) we can produce a detail-enhanced result using Laplacian coating; and (3) we can shape a planar mesh satisfying the two decomposed normal fields for compensating details that was lost during bas-relief modeling, leading to detail-preserving results.

The main contributions of this paper are three-fold:

- We propose a joint weighted least squares algorithm for normal filtering. Different from existing normal filters, the original normal field serves as a shape constraint, and the intermediate normal field by L_0 gradient minimization is considered as the guidance normal field, yielding a piecewise smooth base layer with the overall shape preserved.
- Decomposing a normal field to two layers provides a basis for geometric processing, e.g. detail-preserving bas-relief modeling.
- Existing structure-preserving mesh filters is less suitable than our proposed three-step filter to remove surface details clearly, which best fits the objects with abundant details.

2. Related work

2.1. Mesh filters

Mesh filters are originally developed for smoothing either high-frequency features of surfaces or the corrupted noise [20]. We notice that various filters evolve from the techniques of image denoising, e.g. bilateral filtering [10, 21–25] from [26], anisotropic diffusion filters [27–29] from [30], and L_1/L_0 minimization methods [31, 32] from [33], to name a few. Since a great deal of researches on image denoising serve as a foundation of 3D filters, state-of-the-art methods usually produce quality smoothing/denoising results. However, the aforementioned filters are somewhat less suitable for geometric detail removal, since isotropic filters (e.g. Laplacian filter) commonly result in shape distortion [34], while anisotropic filters (e.g. bilateral filter) cannot eliminate geometric details cleanly. In contrast, we design a three-step filter for effective decomposition of a surface's detail layer and base layer.

2.2. Bas-relief modeling

The work on bas-relief modeling from 3D objects originates from Cignoni *et al* [35]. Later work on this field mainly focuses on preserving salient features, which can be divided into two types. The methods of the first type borrow the idea of high dynamic range (HDR) imaging for compression [36–41], and the methods of the second type are based on surface decomposition and enhancement [38, 42–44].

3. Overview

Without loss of generality, we assume that a 3D surface contains three geometric properties, geometric detail, structure pattern (step edge), and smooth-varying shape. Geometric details represent the detailed appearance of an object, and step edges and smooth-varying shape contribute to control the boundary of geometry features and the overall shape of a local region, respectively. We give a 1D signal decomposition example as an analogy in figure 2.

Under this geometric assumption, we separate a surface into a *detail layer* and a *base layer*, which correspond to geometric details, and the smooth-varying shape plus step edges, respectively. In order to facilitate many geometric processing tasks, the decomposition takes place in the mesh normal field. The decomposition of a normal field is performed by steps of

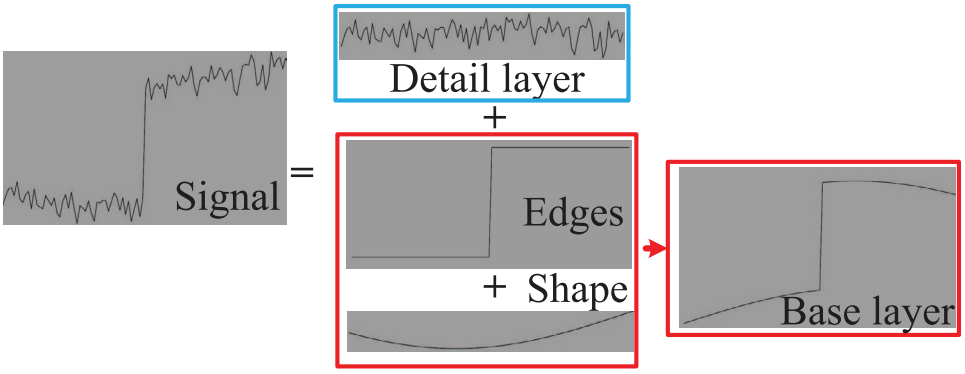

Figure 2. 1D illustration of surface decomposition. Images are courtesy of Shao *et al* [15].

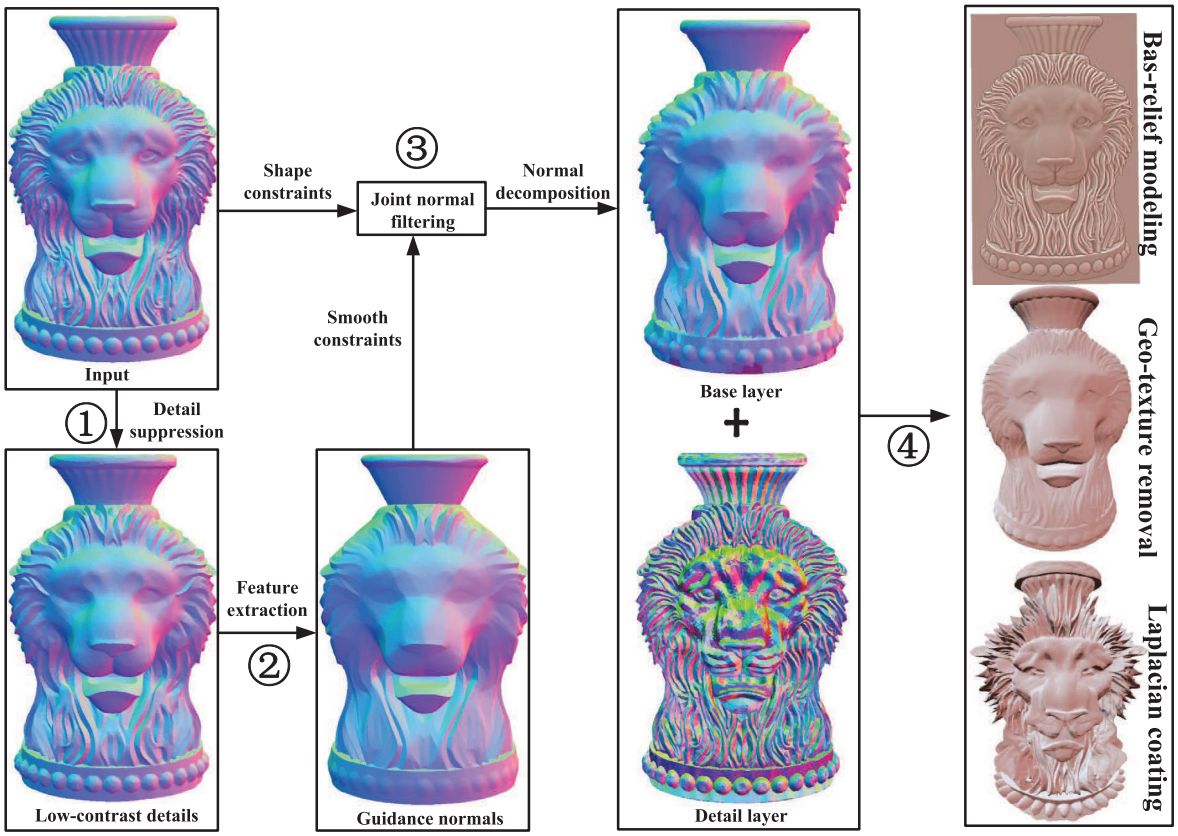

Figure 3. The pipeline of our joint weighted least squares for normal decomposition of 3D measurement surface which is beneficial to many geometric processing tasks.

normal filtering to obtain a base layer, followed by subtracting the base layer from the original surface normal field to acquire a detail layer. The principle behind geometric detail-base decomposition is that normals of salient features are more coherent in local regions while normals of fine details exhibit a wider variety in their directions.

At the top level, we perform the following steps, as shown in figure 3.

(i) By reducing deviations of normals using weighted least squares (WLS), our method suppresses high-contrast detail normals.

(ii) By performing l_0 gradient minimization, our method obtains normals of step edges.

(iii) By performing WLS again but with the original normal field as a shape constraint and the normal field of step edges as a guidance, called *joint normal filtering* in this paper, our method further obtains a base normal field, followed by a subtraction operation to acquire a detail normal field.

(iv) By combining with mesh reconstruction based on the decomposed normal fields, our method suits for many practical meaningful tasks, e.g. bas-relief modeling, geometry texture removal, and Laplacian coating.

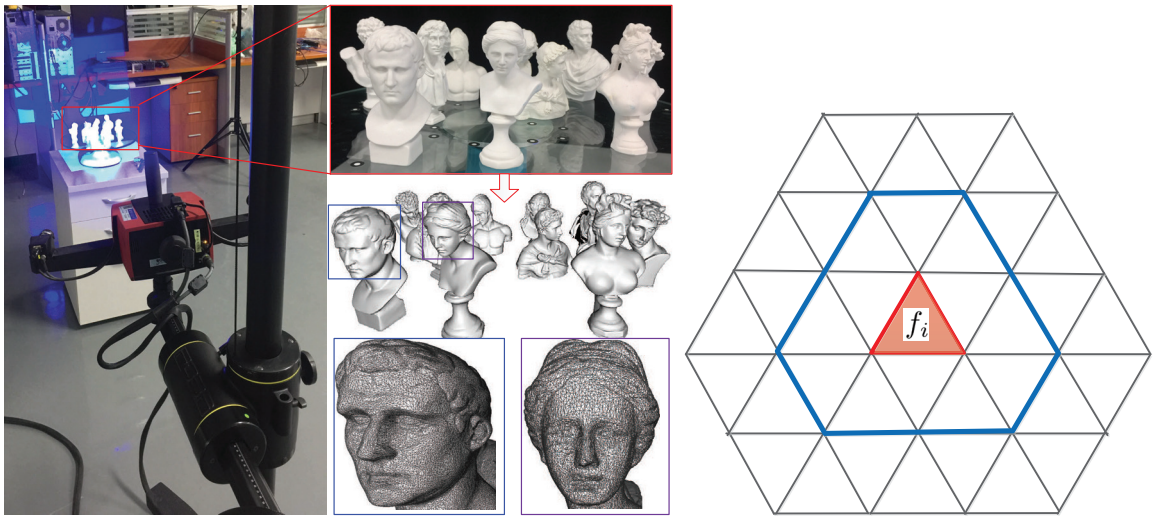

Figure 4. The mesh representation of measurement surface and its local neighborhood. Left: The obtained measurement surface is commonly represented by a watertight triangular mesh for subsequent applications. Right: The 1-ring face neighborhood of f_i (Note that faces within the blue polygon belong to $N_f(i)$).

4. Base-detail decomposition in normal field

Triangular meshes remain a mainstream representation of 3D measurement surfaces (see figure 4(left)) and are perfectly supported by modern graphics hardware. Therefore, we start our surface decomposition from surfaces approximated by triangular meshes. A triangular mesh can be denoted by $M = (V, E, F, N)$. V, E, F, and N represent respectively the sets of vertices, edges, faces, and face normals. We use $N_f(i)$ to describe the faces in the 1-ring face neighborhood of a face $f_i \in F$, which means a set of faces sharing a common vertex or edge with f_i, as shown in figure 4(right).

Given a 3D detail-rich surface mesh $M = (V, E, F, N)$ as input, we aim at obtaining a new normal set N', which is as close as possible to N as to maintain the overall shape of the original mesh, while being as smooth as possible everywhere except across salient features in N. For parametric representation $N : F = F(u, v)$, $(u, v) \in \Omega$, the compromise between the two different objectives can be achieved by seeking the minimum of energy

$$\min_{N'} \int_{\Omega} (N' - N)\mathrm{d}u\mathrm{d}v + \lambda \int_{\Omega} \Phi(N')\mathrm{d}u\mathrm{d}v, \tag{1}$$

where the first term considers resemblance with the original normal field, while the second term measures smoothness of the new normal field. $\lambda > 0$ is a weight used to balance the two terms. That means, the smaller the λ is, the more the new normal set N' is similar to the original normal field N, while the geometric details are hardly removed; while the larger the λ is, the more smoother the new normal set N' is, while the structural patterns would be blurred.

In order to obtain a base normal field N' with details filtered out clearly, we optimize the aforementioned energy in a global way step by step. In specific, (1) we first filter it to suppress fine detail normals to guarantee that their directional deviations are much smaller than those of salient features. This step is achieved by extending weighted least squares (WLS) [16]. (2) We then extract a surface's structure information (step edges) without adverse influences from surface details by l_0 gradient minimization [45]. (3) The obtained normal field in the second step forms a guidance containing structure information about the input model. This normal field then supplies a smoothness constraint, while the original normal field supplies a shape constraint. That is, we decompose the original normal field to a base layer and a detail layer within the joint WLS optimization framework [15]. Since the normal decomposition involves the aforementioned three steps, and each step will produce a new normal field N' as an input to the next step, the sequent normal fields produced in each step may be loosely denoted by N', N'', and N''', where this is not ambiguous.

4.1. Detail normal suppression

Equation (1) can be discretely represented as

$$\min_{N'} \sum_{n_i \in N} \left[(n_i' - n_i)^2 + \lambda_1 (f(n_i')^2) \right], \tag{2}$$

where the goal of data term $(n_i' - n_i)^2$ is to minimize the L_2 distance between N' and N, while the second (smoothness) term is designed to control the smoothness of N'. λ_1 is used to balance the two terms; increasing the value of λ_1 leads to a progressively smoother N'.

Inspired by Laplacian mesh optimization [46], we set $f(n_i')$ to be the weighted Laplacian operator $L(n_i)$, which is equal to the normal difference between face f_i and the weighted average of its neighbors as

$$f(n_i') = s_i L(n_i) = s_i \sum_{f_j \in N_f(i)} w_{ij}(n_j' - n_i'), \tag{3}$$

where w_{ij} is usually the cotan weight [46] of the co-edge e_{ij} between face f_i and face f_j with $\sum w_{ij} = 1$. The parameter s_i is defined in terms of the principle that if face f_i passes through a salient-feature region, a smaller s_i preserves the salient feature;

Figure 5. Shape reconstruction after each step of normal filtering. From left to right: An input merlion model, shape reconstruction results by Wang *et al*'s improved Poisson reconstruction algorithm [11] with normals after the detail suppress stage, the L_0 gradient smoothing stage, and the joint normal filtering stage.

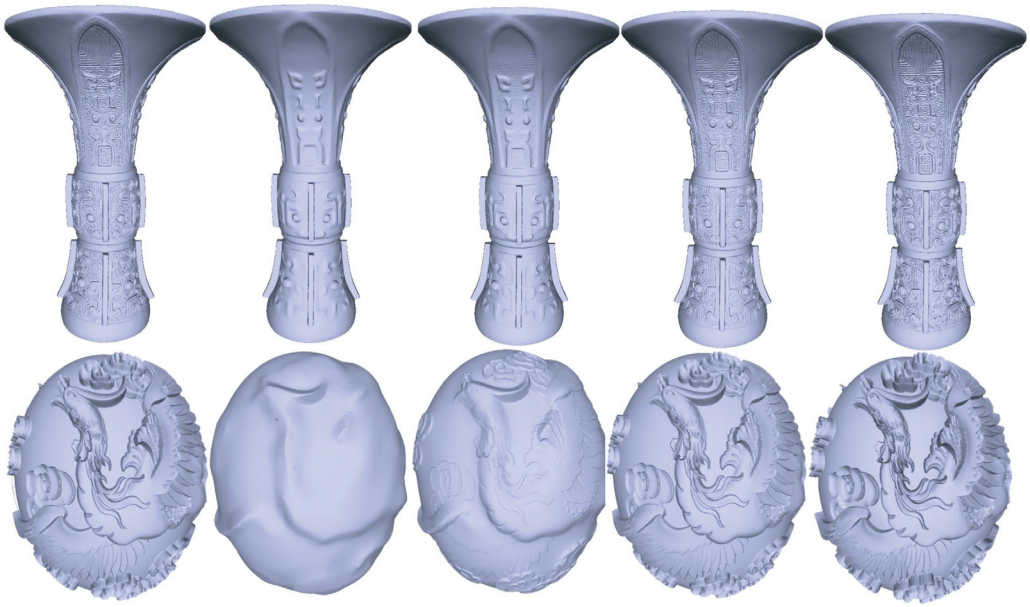

Figure 6. Detail-free smoothing results and their Laplacian coating. From the left column to the right: The input two models, the smoothing results, and the Laplacian coating results with increasing weights (−0.8, −0.2, and 0.4, respectively).

otherwise, a larger s_i will be selected to smooth the surface. According to WLS [16], we set $s_i = (||L(n_i)||^{\alpha} + \epsilon)^{-1}$, where α is a parameter with the values varying within $[1.2, 2]$ which controls the sensitivity to $||L(n_i)||$, and ϵ is assigned a small positive value, e.g. 0.0001, to avoid division by zero.

Equation (2) can be re-written as

$$\min_{N'} \left[(N' - N)^T (N' - N) + \lambda_1 ((N')^T L^T S L N') \right], \quad (4)$$

where S is a diagonal matrix with s_i as the non-zero elements. L is an $m \times m$ (m is the number of mesh faces) Laplacian matrix with values as

$$L_{ij} = \begin{cases} 1, & i = j, \\ -w_{ij}, & e_{ij} \in E, \\ 0, & \text{otherwise.} \end{cases}$$

Equation (4) can be changed to a sparse linear system $(I + \lambda L^T S L)N' = N$, which is solved more efficiently.

4.2. Feature extraction

The L_0 gradient minimization in image smoothing [33] can be extended to mesh vertices [32] and mesh normals [45] by controlling the non-zero normal gradients in a global way. Given a mesh normal field, equation (1) can be discretely formulated as

$$\min_{N''} \sum_{n'_i \in N'} \left[(n''_i - n'_i)^2 + \sum_{f_j \in N_f(i)} \left| n''_i - n''_j \right|_0 \right], \quad (5)$$

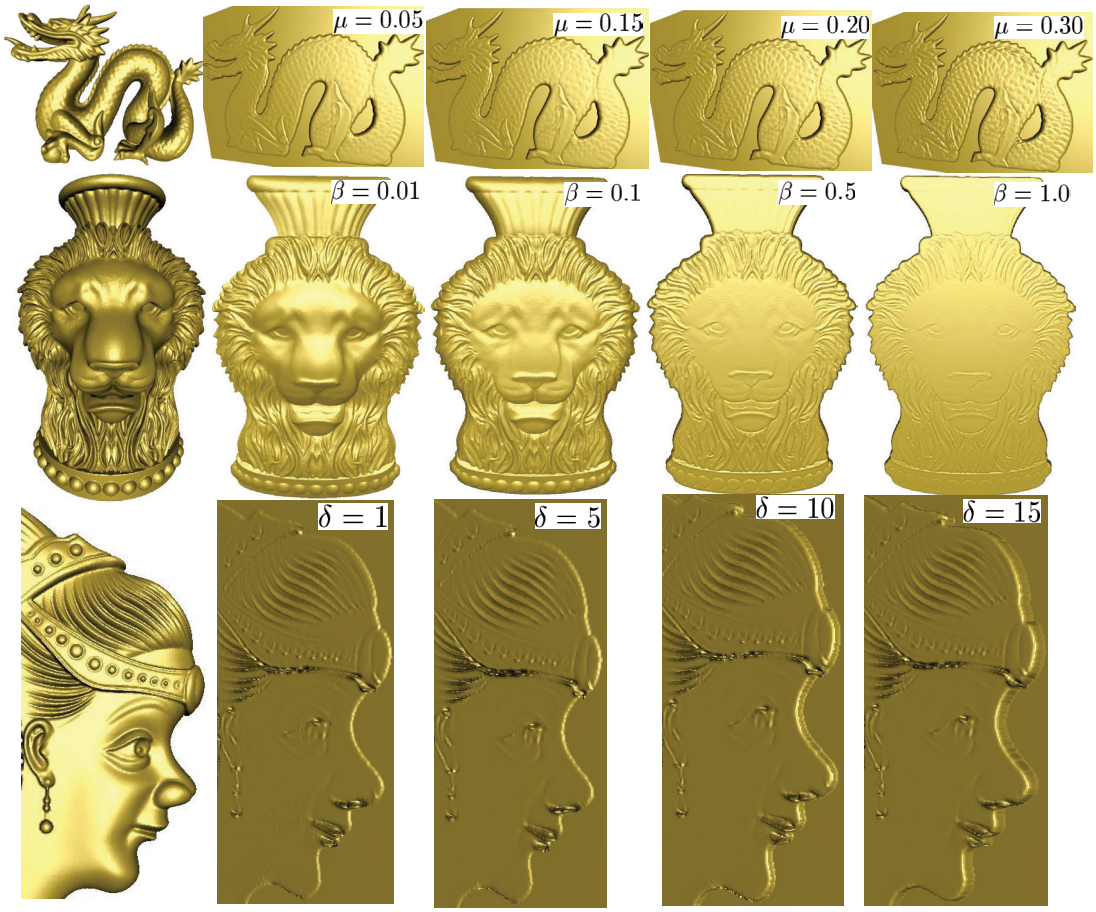

Figure 7. The bas-relief modeling method has three vital parameters. The first row shows that details can be increasingly enhanced by enlarging μ when the other two parameters are fixed, i.e. $\beta = 0.3$, and $\delta = 10$. The second row means that enlarging β can obtain flatter bas-reliefs ($\mu = 0.15, \delta = 12$). The third row illustrates that enlarging δ produces bas-reliefs with higher heights ($\mu = 0.01, \beta = 1$).

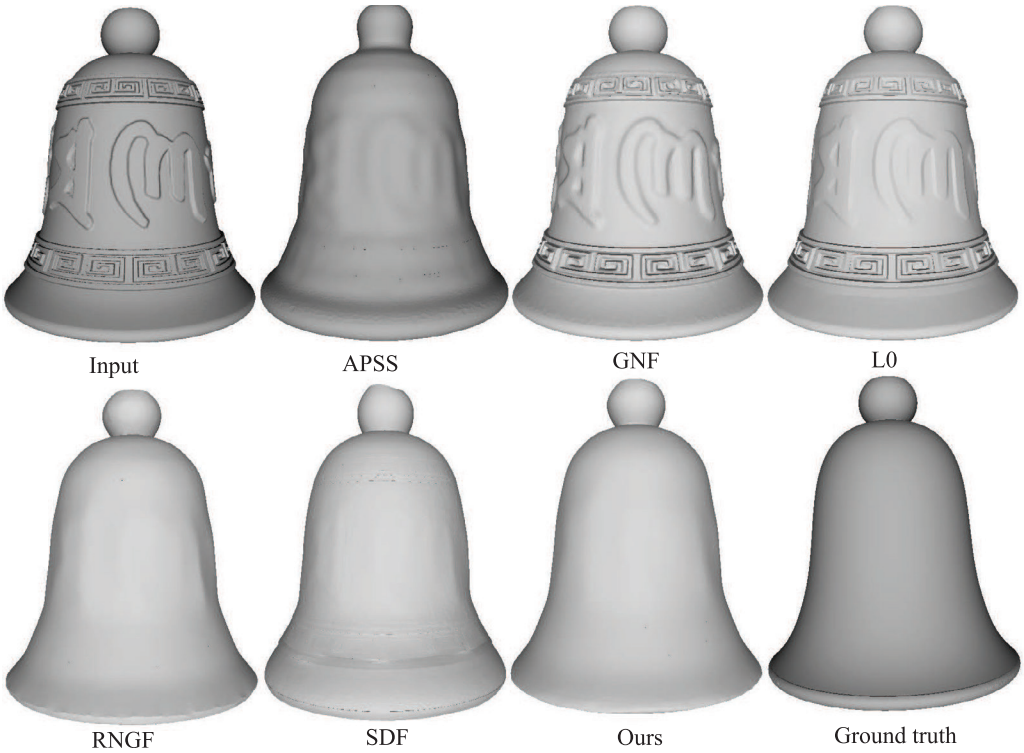

Figure 8. Surface decomposition on Bell. From top-left to bottom right: The input model, and the smoothing results by APSS [47], GNF [48], L0 [32], RNGF [11], SDF [49], and ours, respectively, and the ground-truth model. Some approaches could decompose the surface details clearly while the others may lead to shape shrinkage. Our smoothing result is more similar to the ground-truth model.

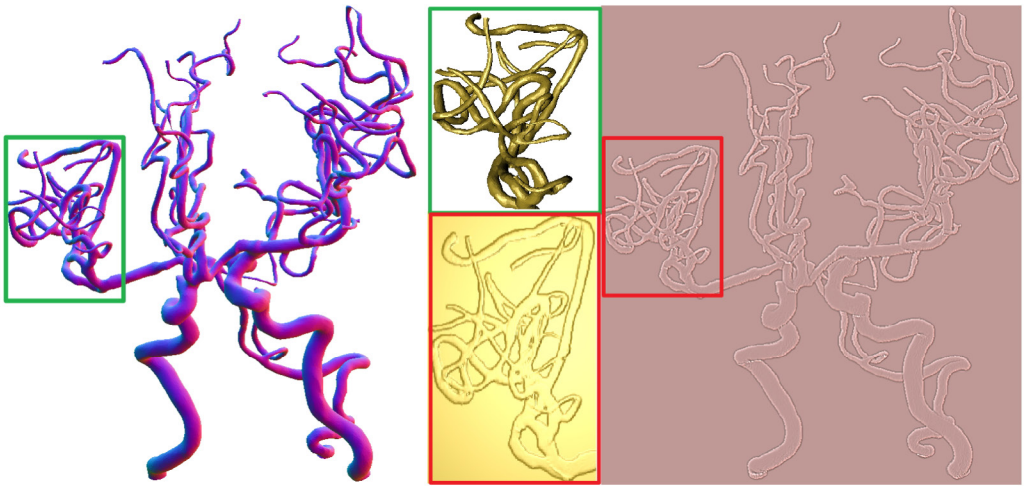

Figure 9. Bas-relief modeling from the model of a complicated vascular tree ($\mu = 0.01$, $\beta = 0.8$, and $\delta = 1$), where detecting depth discontinuity is avoided. The left is input, the right is the created bas-relief, and the middle is their magnified fragments.

Figure 10. Bas-relief modeling of three sculptures. From the left column to the right: For each group, the left is the normal map, and the right is the bas-relief modeling result.

where the data term $(n_i'' - n_i')^2$ is still to minimize the L_2 distance between N'' and N', while the smooth term is the L_0 norm of vector $(n_i'' - n_j'')$ which means the number of non-zero values.

Due to the smooth term in the energy functional above being non-convex and non-differentiable, traditional optimization techniques, such as the gradient descent algorithm, are no longer competent. Xu *et al* [33] give an $L_0 - L_2$ iteration algorithm by introducing a set of auxiliary variables $O = (o_1, o_2, \cdots, o_n)$. Thus, equation (5) can be reformulated as

$$\min_{N'',O} \sum_{n_i' \in N'} \left[(n_i'' - n_i')^2 + \beta \sum_{f_j \in N_f(i)} (n_i'' - n_j'' - o_i)^2 + \phi |o_i|_0 \right], \tag{6}$$

where β is used to control the similarity between the auxiliary variable o_i and $(n_i'' - n_j'')$. Equation (6) can be solved by two steps. First, O is optimized with N' fixed

$$\min_{O} \sum_{n_i' \in N'} \left[\sum_{f_j \in N_f(i)} (n_i'' - n_j'' - o_i)^2 + \frac{\phi}{\beta} |o_i|_0 \right], \tag{7}$$

which is spatially decomposed to a set of single variable function minimization. After this step, O has a high degree of sparsity. Thus, we can next attempt to force N' to match O, i.e. N' is optimized with O fixed

$$\min_{N''} \sum_{n_i' \in N'} \left[(n_i'' - n_i')^2 + \beta \sum_{f_j \in N_f(i)} \lambda_2 (n_i'' - n_j'')^2 \right], \tag{8}$$

which can be solved in a global way by the gradient descent method. After the second step, L_0 minimization (equation (7)) and L_2 minimization (equation (8)) are performed alternately until equation (6) is stable.

Actually, we adopt an improved version proposed in [45] to optimize equation (6), where the energy functional can be optimized in a fused coordinate descent framework, where only one variable is optimized at a time, and the neighboring variables are fused together once their values are equal. More details can be found in [45]. In this way, non-zero gradients will be finally aggregated near sharp features, while zero gradients mainly stay at the region with small scale variations in normal field. Thus, it is feasible to distinguish structure constituents now due to the amplitudes of details having dropped below these of features in section 4.1.

In summary, L_0 smoothing is applied to the detail-suppressed normal field obtained in the previous stage to give a guidance normal field for the next shape recovery stage.

4.3. Joint weighted least squares

By performing WLS again on the surface but with the original normal field N as a shape constraint and the normal field N''

Figure 11. Bas-relief modeling from the models of Buddha, Angel, Armadillo, and Felion, respectively. From the left column to the right: The four inputs, and the results of Weyrich *et al*, Sun *et al*, Ji *et al*, and our improved scheme based on [44], respectively.

of L_0 gradient minimization as a smoothness constraint, called joint WLS, we can finally obtain a base normal field N''', followed by a subtraction operation to acquire a detail normal field.

In detail, the guidance normal field produced in section 4.2 helps to reduce the gap between the output base layer and the original appearance. In this stage, we minimize the energy functional

$$\min_{N'''} \sum_{n_i \in N} \left[(n_i''' - n_i)^2 + \lambda_1 (f(n_i''')^2) \right], \tag{9}$$

where the formulation of $f(n_i''')$ is a little different with the original one in equation (3), that is,

$$f(n_i''') = s_i \sum_{f_j \in N_f(i)} w_{ij}(n_j''' - n_i'''), \tag{10}$$

where s_i in equation (10) depends on the guidance normal field rather than the initial normal field. In detail, $s_i = (||L(n_i'')||^{\alpha} + \epsilon)^{-1}$.

To illustrate the power of the three-step normal filter, we employ the vertex updating scheme, i.e. the improved Poisson reconstruction algorithm in [11] to reconstruct a filtered surface by using the new normal in each stage, i.e. N' from the detail suppress stage, N'' from the L_0 gradient smoothing, and N''' from the joint normal filtering, as shown in figure 5. Furthermore, the geometry details are well removed with their

Table 1. Parameter settings for each method used in figure 11.

Weyrich *et al*	Felion	Armadillo	Budda	Angel
α	6	8	7	5
v_{sil}	0.5	0.35	0.65	0.3
Sun *et al*	Felion	Armadillo	Budda	Angel
B	10 000	10 000	10 000	10 000
m_0	32	32	32	32
n	3	3	3	4
α	5	5	5	5
l	9	16	16	16
Ji *et al*	Felion	Armadillo	Budda	Angel
μ	0.04	0.03	0.05	0.03
θ	10	10	10	10
Ours	Felion	Armadillo	Budda	Angel
λ_1	1.5	1.5	1.5	1.5
λ_2	0.3	0.3	0.3	0.3
α	1.2	1.2	1.2	1.2
μ	0.12	0.15	0.08	0.1
β	0.03	0.05	0.06	0.03
δ	10	10	10	10

overall shape is preserved, and Laplacian coating can be performed on the smoothed results, as shown in figure 6.

5. Results and analysis

We have implemented the JWLS algorithm and the related geometric processing applications by using C++ and OpenGL, where TAUCS is adopted as the linear solver. The experiments have been tested on a PC with a 4.00 GHz Intel core i7 and 32 GB of RAM.

Parameters. Surface normal decomposition, i.e. JWLS, has three parameters, i.e. λ_1, λ_2 and α, which are fixed as $\lambda_1 = 1.5$, $\lambda_2 = 0.3$ and $\alpha = 1.2$ for 3D models, and $\lambda_1 = 2$, $\lambda_2 = 0.45$ and $\alpha = 1.5$ for depth images.

Meanwhile, bas-relief modeling is one of our important applications of surface normal decomposition. Existing normal-based bas-relief modeling techniques can benefit from our decomposed normals by JWLS. We adopt the framework of discrete geometry processing (DGP) proposed in [44] for detail-preserving bas-relief modeling. The DGP framework consists of two steps, i.e. local projection and global blending. In [44], after the step of local projection, bas-relief modeling is achieved by simultaneously optimizing detail preservation (μ), targeted height (δ) and stylization (β) in a global and sparse equation system, called global blending. We here simply explain how to adjust these parameters: A larger μ can prevent to lose a surface's details during compression. A smaller β constructs the roundness style of a surface which keeps the 3D shape heavily, whereas a larger β produces a flatness style. The bas-relief's height is determined by δ. Extensive experiments have shown that $\mu \in [0.01, 1]$, $\beta \in [0.01, 1]$ and $\delta \in [1, 20]$ are good enough to generate desirable bas-relief modeling results. We have demonstrated the modeling results by enlarging one of the parameters in figure 7.

5.1. Surface decomposition

We consider that a 3D surface consists of three geometric properties, i.e. geometric detail, structural pattern, and smooth-varying shape, and propose the joint weighted least squares to filter out the geometric details while preserving the structural pattern. We have found that our JWLS algorithm (we use the improved Poisson reconstruction algorithm in [11] for vertex update) can lead to a promising result which is most similar to the ground-truth model as shown in figure 8 (the parameters of each method are fine tuned to produce the visually best result). Furthermore, we have evaluated the smoothing results numerically in table 2. The numerical results are consistent to the visual results, which illustrates the effectiveness of our approach.

5.2. Normal-based reconstruction

The bas-relief modeling method inherits the advantages of normal-based modeling techniques. For example, it is intrinsically free of depth discontinuity [38], because only the decomposed normal fields are employed. Thus, explicitly detecting these discontinuity regions and removing unused depth intervals at these regions can avoid. Figure 9 illustrates that depth discontinuities of the intricate vascular branches are excluded naturally without explicit detection of the overlapped regions.

5.3. Detail compensation

As known, the surface details are easily lost during a high compression. We can utilize two normal maps to compensate for the loss of details, thanks to the decomposed normal field by JWLS. The parameter μ can prevent to lose surface details. Figure 10 illustrates three sculptures with abundant details and the corresponding modeling results with high compression, where the loss of details are effectively prevented.

We have compared our improved bas-relief modeling approach with the state-of-the-art methods of Weyrich *et al* [36], Sun *et al* [37], Ji *et al* [38], and Schuller *et al* [39]. The visually best results are obtained for each method by fine adjusting their parameters under a same height compression. Figure 11 shows the bas-relief modeling results of four models with abundant details (parameter settings are shown in table 1), and figure 12 shows these results from another view point. Albeit a large height compression, details are still better preserved by our improved approach.

What is more, a slight edge for our approach is that it could still maintain the fine details when the compression is extremely large, see the highlighted parts in figure 13. From figure 14, our approach preserves each model's details better than Ji *et al* [38] when enforced on the 3D model set.

We have also done experiments on depth images. Depth images are a kind of height fields, which also need to be compressed to produce bas-reliefs. We compared with the well-known commercial software ArtCAM. We transform the height fields into normal fields as the input for our method

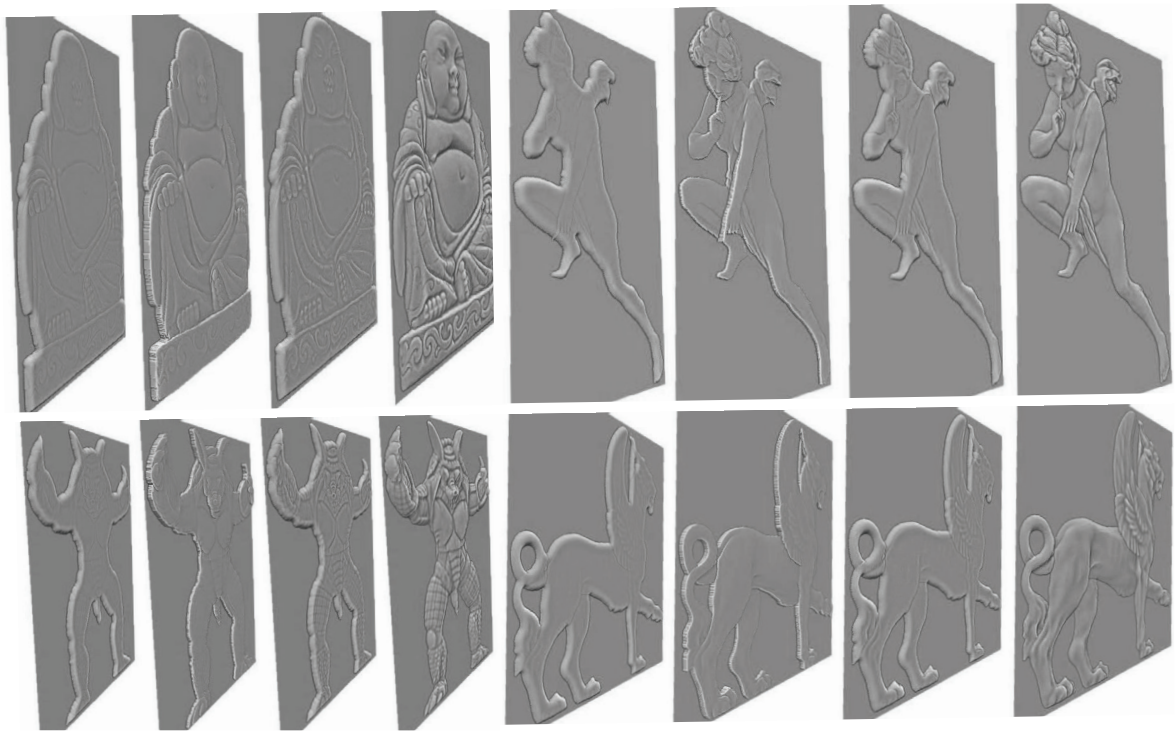

Figure 12. Another view point of the generated bas-reliefs in figure 11.

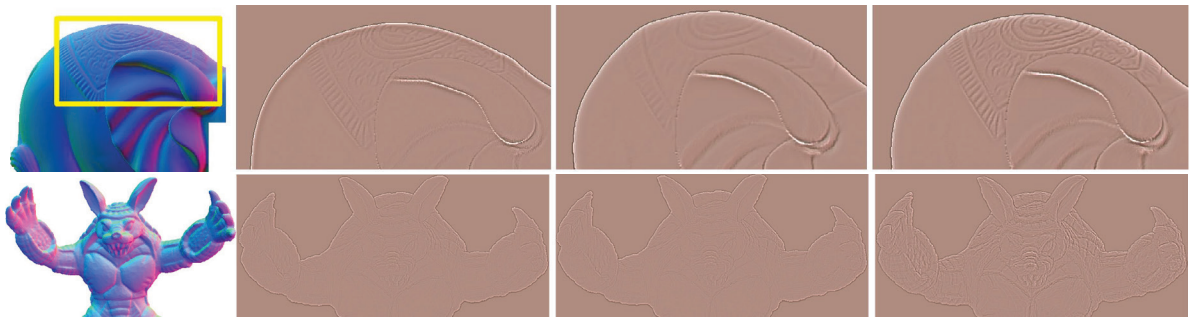

Figure 13. Bas-relief modeling on three models, i.e. Elephant, Armadillo, and Buddha. From the left column to the right: The inputs, the results of Ji *et al* ($\mu = 0.3, \theta = 10$), Schuller *et al*, and ours ($\mu = 0.3, \beta = 0.2, \delta = 10$), respectively.

Figure 14. Bas-relief modeling on the model set. From the left column to the right: A scene of multiple overlapped models, results of Ji *et al*, and ours.

(refer to [38] for the transformation details). Figure 15 illustrates three bas-reliefs of the Chinese style. From the corresponding magnified fragments we know, our improved approach shows better at preserving fine details.

5.4. CNC engraving and 3D printing

We have produced physical bas-relief sculptures by a CNC engraving machine and a 3D printing device. We can see that in figure 16, all details are well preserved which make these sculptures more vivid.

5.5. Computational time

The time performance of our approach has been recorded in table 3 for three typical models. We notice that our method is time-consuming: (1) Three sparse and linear global equations should be solved in normal decomposition. (2) Also,

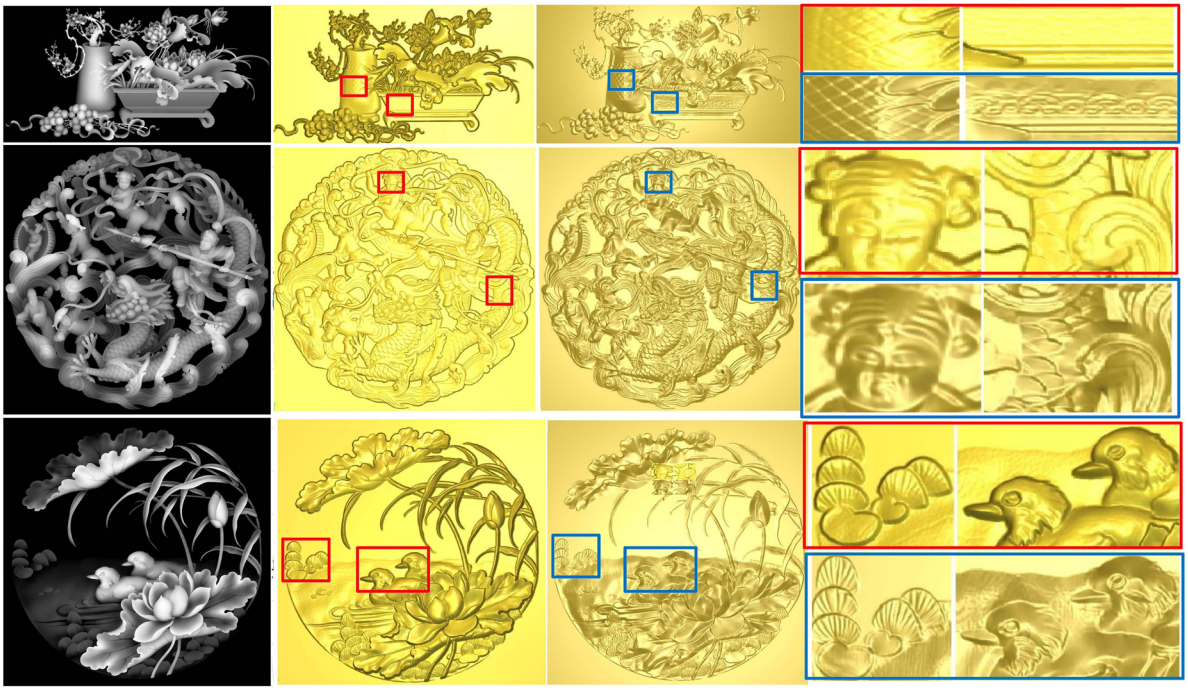

Figure 15. Bas-relief modeling on the scenes of Chinese style. From the left column to the right: the depth images, the results of ArtCAM and our results respectively, and the corresponding magnified fragments for the two methods respectively.

Figure 16. Carving and 3D printing of our modeled bas-reliefs.

Table 2. Numerical analysis of the smoothing results. We measure the vertex-to-vertex distance errors from the smoothing result to the ground-truth model. σ is the standard deviation of distance errors, $D_{\max}$ is the maximal distance error and D_{mean} is the mean distance error (note that the smallest errors are highlighted in bold).

Model	Error	APSS	GNF	ℓ_0	RNGF	SDF	Ours
Bell	σ	0.6350	0.6238	0.6100	0.6367	0.6880	**0.6079**
	$D_{\max}$	2.4240	2.6851	**2.4214**	2.6661	3.2592	2.6638
	D_{mean}	0.7550	0.7880	0.7958	0.7309	0.7437	**0.7263**

Table 3. Timing. For normal decomposition (St1), the numbers denote a model's numbers of the vertices and the faces; for bas-relief modeling (St2), the image resolution is fixed to 1000×900 for all models as suggested by Wei *et al* [44].

Models	St1		St2	Total
Armadillo	25 k, 50 k	1.2 s	66.7 s	67.9 s
Buddha	757 k, 1514 k	100 s	70.5 s	170.5 s
Elephant	171 k, 342 k	16.3 s	67 s	83.3 s

a sparse and linear global equation is solved in bas-relief modeling.

Limitations. The current version of our method does not support the composite modeling, i.e. high relief and bas-relief modeling for different parts of an input model.

6. Conclusion

Mesh geometry processing is a fundamental topic in computer graphics, since 3D optical and laser measurement devices are now widely used to capture the 3D surface. We assume that a 3D surface contains three geometric properties, i.e. geometric detail, structural pattern, and smooth-varying shape, and consider normals as surface signals defined over both the input mesh and the underlying surface of this mesh. Based on such a geometry assumption, we have proposed a novel joint weighted least squares (JWLS) model for 3D surface decomposition. We have introduced three important mesh geometry applications that benefit from our JWLS. For example, digital bas-relief modeling is a hot topic with the increasingly popular 3D scanning and printing techniques. The modeled bas-reliefs should be able to characterize the detailed appearance and intrinsic properties of the input surface. However, most existing bas-relief modeling methods inevitably lose fine details more easily than salient features because of the large compression of 3D models. Fortunately, our JWLS can decompose the original normal field into the detail layer and the base layer, where the detail layer can be used to avoid the loss of detail when performing bas-relief modeling. In future, we will attempt to speed up our approach for real-time applications by modern GPUs.

Acknowledgment

The authors would like to thank the anonymous reviewers for the valuable comments. The work is supported by the National Natural Science Foundation of China under Grant 61502137, the Dean's Research Fund 2016-17 (FLASS/DRF/SFRS-1), Top-Up Fund (TFG-04) and Seed Fund (SFG-10) for General Research Fund/Early Career Scheme and Interdisciplinary Research Scheme of the Dean's Research Fund 2018-19 (FLASS/DRF/IDS-3), Funding Support to General Research Fund Proposal (RG 39/2019-2020R) and the Internal Research Grant (RG 90/2018-2019R) of the Education University of Hong Kong, the Key R&D Program of Guangdong Province, China under Grant 2018B030339001, and the Science and Technology Plan Project of Guangzhou under Grant 201704020141.

ORCID iDs

Mingqiang Wei https://orcid.org/0000-0003-0429-490X

References

[1] Chugui Y, Verkhoglyad A, Poleshchuk A, Korolkov V, Sysoev E and Zavyalov P 2013 3d optical measuring systems and laser technologies for scientific and industrial applications *Meas. Sci. Rev.* **13** 322–8
[2] Zhou Y, Wang W, Luo H and Zhang Y 2019 Virtual preassembly for large steel structures based on bim, plp algorithm, and 3d measurement *Frontiers Eng. Manag.* **6** 1–14
[3] Kilambi S and Tipton S M 2012 Development of an algorithm to measure defect geometry using a 3d laser scanner *Meas. Sci. Technol.* **23** 085604
[4] Wang J, Dai J, Li K S, Wang J, Wei M and Pang M 2019 Cost-effective printing of 3d objects with self-supporting property *Vis. Comput.* **35** 639–51
[5] Ort T, Paull L and Rus D 2018 Autonomous vehicle navigation in rural environments without detailed prior maps *IEEE Int. Conf. on Robotics and Automation* pp 2040–7
[6] Wang J and Yu Z 2011 Surface feature based mesh segmentation *Comput. Graph.* **35** 661–7
[7] Dekkers E and Kobbelt L 2014 Geometry seam carving *Comput.-Aided Des.* **46** 120–8
[8] Botsch M and Sorkine O 2008 On linear variational surface deformation methods *IEEE Trans. Vis. Comput. Graph.* **14** 213–30
[9] Wang J, Gu D, Yu D, Tan C and Zhou L 2012 A framework for 3d model reconstruction in reverse engineering *Comput. Ind. Eng.* **63** 1189–200
[10] Wei M, Yu J, Pang W, Wang J, Qin J, Liu L and Heng P 2015 Bi-normal filtering for mesh denoising *IEEE Trans. Vis. Comput. Graph.* **21** 43–55
[11] Wang P, Fu X, Liu Y, Tong X, Liu S and Guo B 2015 Rolling guidance normal filter for geometric processing *ACM Trans. Graph.* **34** 173
[12] Wei M, Liang L, Pang W, Wang J, Li W and Wu H 2017 Tensor voting guided mesh denoising *IEEE Trans. Autom. Sci. Eng.* **14** 931–45
[13] Wei M, Wang J, Guo X, Wu H, Wang F L and Qin J 2018 Learning-based 3d surface optimization from medical image reconstruction *Opt. Lasers Eng.* **51** 110–8
[14] Wang J and Yu Z 2009 A novel method for surface mesh smoothing: applications in biomedical modeling *Proc. 18th Int. Meshing Roundtable (Salt Lake City, UT, USA, 25–28 October 2009)* pp 195–210
[15] Shao P, Ding S, Ma L, Wu Y and Wu Y 2015 Edge-preserving image decomposition via joint weighted least squares *Comput. Vis. Media* **1** 37–47
[16] Farbman Z, Fattal R, Lischinski D and Szeliski R 2008 Edge-preserving decompositions for multi-scale tone and detail manipulation *ACM Trans. Graph.* **27** 1–10
[17] Bhat P, Zitnick C L, Cohen M F and Curless B 2010 Gradientshop: a gradient-domain optimization framework for image and video filtering *ACM Trans. Graph.* **29**
[18] Liu W, Chen X, Shen C, Liu Z and Yang J 2017 Semi-global weighted least squares in image filtering *The IEEE Int. Conf. on Computer Vision* pp 5862–70
[19] Liang L, Wei M, Szymczak A, Petrella A, Xie H, Qin J, Wang J and Wang F L 2018 Nonrigid iterative closest points for registration of 3d biomedical surfaces *Opt. Lasers Eng.* **100** 141–54

[20] Wang J, Zhang X and Yu Z 2012 A cascaded approach for feature-preserving surface mesh denoising *Comput. Aided Des.* **44** 597–610
[21] Shachar F, Iddo D and Daniel C-O 2003 Bilateral mesh denoising *ACM Trans. Graph.* **22** 950–3
[22] Jones T R, Durand F and Desbrun M 2003 Non-iterative, feature-preserving mesh smoothing *ACM Trans. Graph.* **22** 943–9
[23] Zheng Y, Fu H, Au O K-C and Tai C-L 2011 Bilateral normal filtering for mesh denoising *IEEE Trans. Vis. Comput. Graph.* **17** 1521–30
[24] Wei M, Shen W, Qin J, Wu J, Wong T-T and Heng P-A 2013 Feature-preserving optimization for noisy mesh using joint bilateral filter and constrained laplacian smoothing *Opt. Lasers Eng.* **103** 1223–34
[25] Yu J, Wei M, Qin J, Wu J and Heng P-A 2014 Feature-preserving mesh denoising via normal guided quadric error metrics *Opt. Lasers Eng.* **62** 57–68
[26] Tomasi C and Manduchi R 1998 Bilateral filtering for gray and color images *Proc. 6th Int. Conf. on Computer Vision* pp 839–46
[27] Bajaj C and Xu G 2003 Anisotropic diffusion on surfaces and functions on surfaces *ACM Trans. Graph.* **22** 4–32
[28] Clarenz U, Diewald U and Rumpf M 2000 Anisotropic geometric diffusion in surface processing *IEEE Vis.* pp 397–405
[29] Ouafdi A E and Ziou D 2008 A global physical method for manifold smoothing *Proc. Shape Model. Int.* pp 11–7
[30] Perona P and Malik J 1990 Scale-space and edge detection using anisotropic diffusion *Proc. Shape Model. Int.* **12** 629–39
[31] Wang R, Yang Z, Liu L, Deng J and Chen F 2014 Decoupling noise and features via weighted l1-analysis compressed sensing *ACM Trans. Graph.* **33** 18
[32] He L and Schaefer S 2013 Mesh denoising via L_0 minimization *SIGGRAPH* **32** 64
[33] Xu L, Lu C, Xu Y and Jia J 2011 Image smoothing via L_0 gradient minimization *ACM Trans. Graph.* **30** 174
[34] Wang J and Yu Z 2011 Quality mesh smoothing via local surface fitting and optimum projection *Graph. Models* **73** 127–39
[35] Cignoni P, Montani C and Scopigno R 1997 Computer-assisted generation of bas-and high-reliefs *J. Graph. GPU Game Tools* **2** 15–28
[36] Weyrich T, Deng J, Barnes C, Rusinkiewicz S and Finkelstein A 2007 Digital bas-relief from 3d scenes *ACM Trans. Graph.* **26** 32
[37] Sun X, Rosin P L, Martin R R and Langbein F C 2009 Bas-relief generation using adaptive histogram equalization *IEEE Trans. Vis. Comput. Graph.* **15** 642–53
[38] Ji Z, Ma W and Sun X 2014 Bas-relief modeling from normal images with intuitive styles *IEEE Trans. Vis. Comput. Graph.* **20** 675–85
[39] Schuller C, Panozzo D and Sorkine-Hornung O 2014 Appearance-mimicking surfaces *ACM Trans. Graph.* **33** 216:1–216:10
[40] Zhang Y, Zhou Y, Li X, Liu H and Zhang L 2015 Bas-relief generation and shape editing through gradient-based mesh deformation *IEEE Trans. Vis. Comput. Graph.* **21** 328–38
[41] Liu Y, Ji Z, Liu Z and Wu X 2016 Stylized design of bas-relief based on normal field *J. Comput.-Aided Des. Comput. Graph.* **28** 2120–7
[42] Kerber J, Tevs A, Belyaev A G, Zayer R and Seidel H 2010 Real-time generation of digital bas-reliefs *Comput.-Aided Des. Appl.* **7** 465–78
[43] Zhang Y, Zhou Y, Zhao X and Yu G 2013 Real-time bas-relief generation from a 3d mesh *Graph. Models* **75** 2–9
[44] Wei M, Tian Y, Pang W-M, Wang C C, Pang M, Wang J, Qin J and Heng P-A 2018 Bas-relief modeling from normal layers *IEEE Trans. Vis. Comput. Graph.* **25** 1651–65
[45] Cheng X, Zeng M and Liu X 2014 Feature-preserving filtering with l_0 gradient minimization *Comput. Graph.* **38** 150–7
[46] Nealen A, Igarashi T, Sorkine O and Alexa M 2006 Laplacian mesh optimization *Proc. 4th Int. Conf. on Computer Graphics and Interactive Techniques in Australasia and Southeast Asia* pp 381–9
[47] Guennebaud G and Gross M H 2007 Algebraic point set surfaces *ACM Trans. Graph.* **26** 23
[48] Zhang W, Deng B, Zhang J, Bouaziz S and Liu L 2015 Guided mesh normal filtering *Comput. Graph. Forum* **34** 23–34
[49] Zhang J, Deng B, Hong Y, Peng Y, Qin W and Liu L 2018 Static/dynamic filtering for mesh geometry *IEEE Trans. Vis. Comput. Graphics* **25** 1774–87